Inorganic Chemistry

Article

pubs.acs.org/IC

Diversity of Lanthanide(III)−Organic Extended Frameworks with a 4,8-Disulfonyl-2,6-naphthalenedicarboxylic Acid Ligand: Syntheses, Structures, and Magnetic and Luminescent Properties

Qing-Yan Liu,*[,†,‡] Wu-Fang Wang,[†] Yu-Ling Wang,[†] Zeng-Mei Shan,[†] Ming-Sheng Wang,[‡] and Jinkui Tang*[,§]

[†]College of Chemistry and Chemical Engineering, Jiangxi Normal University, Nanchang, Jiangxi 330022, P. R. China

[‡]State Key Laboratory of Structural Chemistry, Fujian Institute of Research on the Structure of Matter, Chinese Academy of Sciences, Fuzhou, Fujian 350002, P. R. China

[§]State Key Laboratory of Rare Earth Resource Utilization, Changchun Institute of Applied Chemistry, Chinese Academy of Sciences, Changchun 130022, P. R. China

Supporting Information

ABSTRACT: A sulfonate−carboxylate ligand, 4,8-disulfonyl-2,6-naphthalenedicarboxylic acid (H_4-DSNDA), and eight new lanthanide coordination polymers $\{[Pr_4(OH)_4(DSNDA)_2(H_2O)_{12}](H_2O)_{10}\}_n$ (**1**), $[Ln(H_2\text{-}DSNDA)_{0.5}(DSNDA)_{0.5}(H_2O)_5]_n$ (Ln = La(**2**), Nd(**3**), Sm(**4**), Eu(**5**), Gd(**6**), and Dy(**7**)), and $\{[Er(H\text{-}DSNDA)(H_2O)_4](H_2O)\}_n$ (**8**) have been synthesized. Detailed crystal structures of these compounds have been investigated. Compound **1** has a 3D framework featuring the unique cubane-shaped $[Pr_4(\mu_3\text{-}OH)_4]$ clusters and is a binodal 4,8-connected network with $(4^{16}\cdot6^{12})(4^4\cdot6^2)_2$ topology. Compounds **2**−**7** are isostructural and have 2D layered structures. Compound **8** is also a 2D layer but belongs to different structural types. The luminescence behavior of compound Eu(**5**) shows that the π-rich aromatic organic ligands efficiently transfer the absorbed light energy to the Eu(III) ions, thus enhancing the overall luminescent properties of compound Eu(**5**). The magnetic properties of all compounds except for the diamagnetic La(**2**) compound have been investigated. In addition, elemental analysis, IR spectra, and thermogravimetric analysis of these compounds are also described.

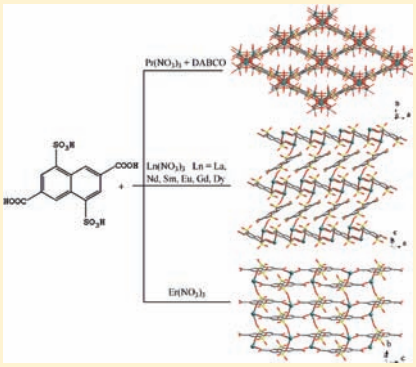

INTRODUCTION

Coordination polymers (CPs) or metal−organic frameworks (MOFs) from metal ions or metal clusters with multifunctional organic ligands are currently of great interest due to their potential applications in catalysis, molecular magnets, photoluminescence, adsorption, and phase separation, as well as their aesthetically appealing structural topology.[1] To date, many of the efforts have so far been devoted to the study of transition-metal-based coordination polymers. The lanthanide analogues are also highly sought after because the lanthanide ions possess a high coordination number and flexible coordination geometry that can afford structural diversity.[2] In addition, lanthanide compounds can display distinct intrinsic optical and magnetic properties that are much different from those of transition-metal compounds.[3,4]

On the other hand, the organic ligand plays a vital role in the synthesis of the coordination polymers. Among these reported organic ligands, carboxylate ligands are some of the most successful functional ligands. Comparing with carboxylate ligands, organosulfonate ligands have received much less attention.[5] The sulfonate group with three potential oxygen coordination sites, which is a weak ligating group, has more flexible coordination modes, which can form highly flexible frameworks displaying interesting solid state dynamics[6] and hydrogen-bonded networks through extensive hydrogen bonds.[7] In our work on the synthesis of functionalized coordination polymers we are interested in the multifunctional sulfonate−carboxylate ligands.[8] The sulfonate−carboxylate ligand with a strong coordination ability of the carboxylate group and weak coordination ability of the sulfonate group simultaneously has received increasing interest recently. 5-Sulfoisophthalic acid,[9] 2-sulfoterephthalic acid,[10] 3-sulfobenzoic acid,[11] and 4-sulfobenzoic acid[12] have been employed to construct coordination polymers with diverse structures and interesting properties. Nevertheless, there are still relatively few examples of coordination polymers based on sulfonate−carboxylate ligands to date. Herein a sulfonate−carboxylate ligand, 4,8-disulfonyl-2,6-naphthalenedicarboxylic acid (H_4-DSNDA), has been prepared. The H_4-DSNDA ligand with a π-rich naphthalene backbone and two carboxyl and two sulfonyl functional groups is an effective component in the design of a diverse range of coordination polymers. However, the coordination chemistry the H_4-DSNDA ligand is seldom

Received: November 1, 2011
Published: January 30, 2012

dx.doi.org/10.1021/ic2023727 | Inorg. Chem. 2012, 51, 2381−2392

investigated. To the best of our knowledge, only one compound with H_4-DSNDA ligand has been reported very recently, wherein a molecular supertetrahedron $[Fe_{16}O_4(SO_4)_{12}(DSNDA)_6]$ based on the mixed-valence tetranuclear $[Fe_3^{3+}Fe^{2+}(\mu_3\text{-}O)(\mu_3\text{-}SO_4)_3(CO_2)_3]$ clusters is isolated.[13] In this contribution, a series of H_4-DSNDA-based lanthanide coordination polymers has been synthesized and characterized. The magnetic behavior of all compounds has been studied with the exception of the diamagnetic La(III) compound. The luminescence properties of the Eu(III) compound have also been investigated in detail.

EXPERIMENTAL SECTION

Chemicals. All chemicals were of reagent grade and used as commercially obtained. The starting material 4,8-disulfonyl-2,6-naphthalenedicarboxylic acid (H_4-DSNDA) was prepared following the previously reported procedure.[14]

Physical Measurements. Elemental analyses were carried out on an Elementar Vario EL III analyzer, and IR spectra (KBr pellets) were recorded on PerkinElmer Spectrum One. Fluorescent spectra were measured at room temperature with a single-grating Edinburgh EI920 fluorescence spectrometer equipped with a 450-W Xe lamp, an nF900 lamp, and a R928P PMT detector. Magnetic measurements were carried out on crystalline samples with a Quantum Design MPMS-5 magnetometer. The thermogravimetric measurements were performed with a Netzsch STA449C apparatus under a nitrogen atmosphere with a heating rate of 10 °C/min from 25 to 600 °C.

Synthesis of the H_4-DSNDA Ligand (Scheme 1). One gram (4.63 mmol) of naphthalene-2,6-dicarboxylic acid was slowly added to

Scheme 1. Preparation of the H_4-DSNDA Ligand

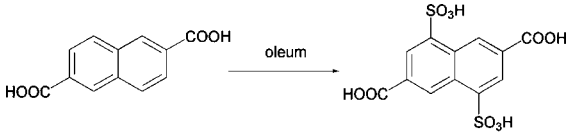

H_4-DSNDA

a 25 mL three-neck flask containing 5 mL of fuming sulfuric acid (SO_3, 20 wt %) under stirring. Then the reaction mixture was vigorously stirred at 150 °C for 6 h. After cooling to room temperature, the mixture was dissolved in deionized water and the acid H_4-DSNDA was precipitated using concentrated HCl. The product was collected by filtration and dried at 100 °C. Yield: 1.49 g (~86%) based on naphthalene-2,6-dicarboxylic acid. IR spectrum (cm^{-1}, KBr pellet): 1243 (s), 1194 (s), 1112 (m), and 1048 (s) (O═S═O of $-SO_3H$ group); 615 (s) (C−S). ^1H NMR (400 MHz, DMSO-d_6, δ, ppm): 9.59 (s, the hydrogen atoms at the ortho positions to $-SO_3H$ groups) and 8.49 (s, the hydrogen atoms at the para positions to $-SO_3H$ groups).

Synthesis of $\{[Pr_4(OH)_4(DSNDA)_2(H_2O)_{12}](H_2O)_{10}\}_n$ (1). A mixture of $Pr(NO_3)_3{\cdot}6H_2O$ (0.448 g, 0.1 mmol), 4,8-disulfonyl-2,6-naphthalenedicarboxylic acid (0.0376 g, 0.1 mmol), and 1,4-diazabicyclo[2.2.2]octan (0.0221 g, 0.1 mmol) in a 1:1:1 molar ratio in 10 mL of H_2O (pH = 5) was introduced into a Parr Teflon-lined stainless steel vessel (25 mL). The vessel was sealed and heated to 140 °C. The temperature was held for 4 days, and then the mixture was cooled naturally to obtain colorless crystals of **1**. Colorless crystalline product was filtered, washed with H_2O, and dried at ambient temperature. Yield: 0.014 g, 33% based on Pr. Anal. Calcd for $C_{24}H_{56}O_{46}S_4Pr_4$ (1772.57): C, 16.26; H, 3.18. Found: C, 16.18; H, 3.11. IR spectrum (cm^{-1}, KBr pellet): 3413 (m), 1641 (s), 1612 (s), 1550 (s), 1479 (m), 1418 (vs), 1369 (m), 1228 (w), 1178 (vs), 1064 (vs), 946 (w), 857 (w), 820 (w), 789 (m), 719 (w), 604 (m), 546 (w), 515 (w).

Synthesis of $[Ln(H_2\text{-}DSNDA)_{0.5}(DSNDA)_{0.5}(H_2O)_5]_n$ (Ln = La(2), Nd(3), Sm(4), Eu(5), Gd(6), Dy(7)). All six compounds were prepared by the same method as follows: A mixture of $Ln(NO_3)_3{\cdot}6H_2O$ (Ln = La, Nd, Sm, Eu, Gd, and Dy, 0.1 mmol) and 4,8-disulfonyl-2,6-naphthalenedicarboxylic acid (0.0376 g, 0.1 mmol) in a 1:1 molar ratio in 10 mL of H_2O (pH = 3) was introduced into a Parr Teflon-lined stainless steel vessel (25 mL). The vessel was sealed and heated to 140 °C. The temperature was held for 4 days and then the mixture was cooled naturally to obtain colorless crystals. Crystalline product was filtered, washed with H_2O, and dried at ambient temperature. Yield: 0.011 g, 19% for **2**; 0.015 g, 25% for **3**; 0.009 g, 16% for **4**; 0.017 g, 28% for **5**; 0.019 g, 32% for **6**; 0.008 g, 13% for **7**; based on Ln). Anal. Calcd for $C_{12}H_{15}O_{15}S_2La$ (**2**) (602.27): C, 23.93; H, 2.51. Found: C, 23.85; H, 2.31. IR spectrum (cm^{-1}, KBr pellet): 3416 (s), 1704 (s), 1639 (m), 1611 (m), 1550 (vs), 1478 (w), 1415 (vs), 1368 (m), 1135 (m), 1176 (vs), 1053 (s), 928 (w), 857 (w), 819 (m), 804 (m), 788 (m), 719 (w), 656 (w), 604 (m), 515 (m). Anal. Calcd for $C_{12}H_{15}O_{15}S_2Nd$ (**3**) (607.60): C, 23.72; H, 2.49. Found: C, 23.67; H, 2.44. IR spectrum (cm^{-1}, KBr pellet): 3419 (s), 1700 (s), 1639 (m), 1617 (m), 1560 (s), 1423 (w), 1401 (s), 1360 (m), 1156 (vs), 1067 (s), 951 (m), 860 (m), 791 (w), 619 (w), 546 (w), 604 (m), 516 (m). Anal. Calcd for $C_{12}H_{15}O_{15}S_2Sm$ (**4**) (613.71): C, 23.48; H, 2.46. Found: C, 23.41; H, 2.35. IR spectrum (cm^{-1}, KBr pellet): 3412 (s), 1703 (s), 1642 (m), 1613 (m), 1552 (vs), 1479 (w), 1421 (vs), 1371 (m), 1140 (m), 1180 (vs), 1055 (s), 927 (w), 857 (w), 820 (m), 805 (m), 791 (m), 719 (w), 604 (m), 514 (m). Anal. Calcd for $C_{12}H_{15}O_{15}S_2Eu$ (**5**) (615.32): C, 23.42; H, 2.46. Found: C, 23.31; H, 2.39. IR spectrum (cm^{-1}, KBr pellet): 3412 (s), 1703 (s), 1644 (m), 1614 (m), 1553 (vs), 1478 (w), 1418 (vs), 1372 (m), 1142 (m), 1192 (vs), 1055 (s), 925 (w), 856 (w), 821 (m), 806 (m), 791 (m), 719 (w), 608 (m), 514 (m). Anal. Calcd for $C_{12}H_{15}O_{15}S_2Gd$ (**6**) (620.61): C, 23.22; H, 2.44. Found: C, 23.25; H, 2.35. IR spectrum (cm^{-1}, KBr pellet): 3415 (s), 1700 (s), 1652 (m), 1615 (m), 1599 (vs), 1456 (w), 1419 (vs), 1373 (m), 1160 (vs), 1075 (s), 947 (w), 859 (m), 822 (w), 792 (m), 708 (w), 604 (w), 547 (m), 517 (m). Anal. Calcd for $C_{12}H_{15}O_{15}S_2Dy$ (**7**) (625.86): C, 23.03; H, 2.42. Found: C, 22.98; H, 2.37. IR spectrum (cm^{-1}, KBr pellet): 3422 (s), 1703 (s), 1642 (m), 1615 (m), 1557 (vs), 1480 (w), 1427 (s), 1373 (m), 1130 (m), 1180 (vs), 1137 (s), 1069 (s), 998 (w), 955 (w), 864 (w), 822 (m), 806 (w), 793 (m), 718 (w), 606 (m), 516 (m).

Synthesis of $\{[Er(H\text{-}DSNDA)(H_2O)_4](H_2O)\}_n$ (8). A mixture of $Er(NO_3)_3{\cdot}6H_2O$ (0.0461 g, 0.1 mmol) and 4,8-disulfonyl-2,6-naphthalenedicarboxylic acid (0.0376 g, 0.1 mmol) in a 1:1 molar ratio in 10 mL of H_2O (pH = 3) was introduced into a Parr Teflon-lined stainless steel vessel (25 mL). The vessel was sealed and heated to 140 °C. The temperature was held for 4 days, and then the mixture was cooled naturally to obtain pink crystals. Pink crystalline product was filtered, washed with H_2O, and dried at ambient temperature. Yield: 0.014 g, 23% based on Er. Anal. Calcd for $C_{12}H_{15}O_{15}S_2Er$ (630.62): C, 22.86; H, 2.40. Found: C, 22.81; H, 2.33. IR spectrum (cm^{-1}, KBr pellet): 3429 (s), 1685 (s), 1644 (m), 1603 (m), 1409 (vs), 1373 (w), 1277 (m), 1194 (vs), 1162 (s), 1115 (w), 1088 (w), 1054 (s), 1025 (w), 920 (w), 861 (w), 810 (w), 779 (w), 763 (m), 699 (w), 640 (w), 607 (s), 530 (w).

X-ray Crystallography. X-ray diffraction data of compounds **1**−**8** were collected on a Bruker Apex II CCD diffractometer equipped with graphite-monochromated Mo Kα radiation (λ = 0.71073 Å). Data reduction was performed using SAINT and corrected for Lorentz and polarization effects. Adsorption corrections were applied using the SADABS routine.[15] Structures were solved by direct methods and successive Fourier difference syntheses and refined by the full-matrix least-squares method on F^2 (SHELXTL Version 5.1).[16] All non-hydrogen atoms are refined with anisotropic thermal parameters. Hydrogen atoms were assigned to calculated positions. Water hydrogen atoms for compound **1** could not be located in the difference Fourier map. The R_1 values are defined as $R_1 = \Sigma||F_o| - |F_c||/\Sigma|F_o|$ and $wR_2 = \{\Sigma[w(F_o^2 - F_c^2)^2]/\Sigma[w(F_o^2)^2]\}^{1/2}$. Details of the crystal parameters, data collection, and refinement are summarized in Tables 1 and 2, and selected bond lengths and bond angles are listed in Table S1, Supporting Information.

dx.doi.org/10.1021/ic2023727 | Inorg. Chem. 2012, 51, 2381−2392

Table 1. Crystallographic Data for Compounds 1−4[a]

	Pr(1)	La(2)	Nd(3)	Sm(4)
formula	$C_{12}H_{28}O_{23}S_2Pr_2$	$C_{12}H_{15}O_{15}S_2La$	$C_{12}H_{15}O_{15}S_2Nd$	$C_{12}H_{15}O_{15}S_2Sm$
fw	886.28	602.27	607.60	613.71
temp (*K*)	296(2)	296(2)	296(2)	296(2)
cryst syst	orthorhombic	triclinic	triclinic	triclinic
space group	*Cmcm*	*P*−1	*P*−1	*P*−1
Z	8	2	2	2
a (Å)	21.859(4)	7.0471(4)	7.02170(10)	7.013(6)
b (Å)	11.5288(18)	10.9758(5)	10.9089(2)	10.917(9)
c (Å)	21.861(3)	12.2698(6)	12.1681(2)	12.119(10)
α (deg)	90	84.2890(10)	84.2090(10)	95.919(10)
β (deg)	90	76.7700(10)	76.6360(10)	103.259(10)
γ (deg)	90	89.5200(10)	89.8110(10)	90.014(10)
V (Å^3)	5509.1(16)	919.16(8)	902.00(3)	898.1(13)
D_{calcd} (g·cm^{-3})	2.137	2.176	2.237	2.270
μ (mm^{-1})	3.742	2.633	3.193	3.585
no. of reflns collected	11 187	8674	12 175	8044
independent reflns	3540	4439	4155	4432
obsd reflns ($I > 2\sigma(I)$)	2437	4325	3930	3935
F(000)	3472	592	598	602
R[int]	0.0839	0.0192	0.0315	0.0525
R_1 ($I > 2\sigma(I)$)	0.0551	0.0194	0.0251	0.0591
wR_2 (all data)	0.1389	0.0503	0.0594	0.1684

[a] $R_1 = \Sigma||F_o| - |F_c||/\Sigma|F_o|$ and $wR_2 = \{\Sigma[w(F_o^2 - F_c^2)^2]/\Sigma[w(F_o^2)^2]\}^{1/2}$.

Table 2. Crystallographic Data for Compounds 5−8[a]

	Eu(5)	Gd(6)	Dy(7)	Er(8)
formula	$C_{12}H_{15}O_{15}S_2Eu$	$C_{12}H_{15}O_{15}S_2Gd$	$C_{12}H_{15}O_{15}S_2Dy$	$C_{12}H_{15}O_{15}S_2Er$
fw	615.32	620.61	625.86	630.62
temp (*K*)	296(2)	296(2)	296(2)	296(2)
cryst syst	triclinic	triclinic	triclinic	monoclinic
space group	*P*−1	*P*−1	*P*−1	$P2_1/m$
Z	2	2	2	2
a (Å)	7.0140(18)	7.00660(10)	7.00090(10)	10.871(2)
b (Å)	10.872(3)	10.8551(2)	10.83150(10)	6.7535(12)
c (Å)	12.083(3)	12.0541(2)	12.01550(10)	11.859(2)
α (deg)	84.193(3)	84.2160(10)	95.8500(10)	90
β (deg)	76.515(3)	76.4690(10)	103.6300(10)	96.180(2)
γ (deg)	89.976(3)	90.0340(10)	90.1370(10)	90
V (Å^3)	891.1(4)	886.54(3)	880.538(17)	865.6(3)
D_{calcd} (g·cm^{-3})	2.293	2.325	2.361	2.420
μ (mm^{-1})	3.838	4.060	4.565	5.175
no. of reflns collected	6522	15 255	15 299	5431
independent reflns	3697	4111	4053	2258
obsd reflns ($I > 2\sigma(I)$)	3394	3947	3701	2020
F(000)	604	606	610	614
R[int]	0.0257	0.0326	0.0341	0.0371
R_1 ($I > 2\sigma(I)$)	0.0255	0.0286	0.0246	0.0318
wR_2 (all data)	0.0600	0.0892	0.0631	0.0752

[a] $R_1 = \Sigma||F_o| - |F_c||/\Sigma|F_o|$ and $wR_2 = \{\Sigma[w(F_o^2 - F_c^2)^2]/\Sigma[w(F_o^2)^2]\}^{1/2}$.

RESULTS AND DISCUSSION

Syntheses. Compound $\{[Pr_4(OH)_4(DSNDA)_2(H_2O)_{12}]\cdot(H_2O)_{10}\}_n$ (**1**) was surprisingly obtained by hydrothermal reaction of $Pr(NO_3)_3$ and H_4-DSNDA in the presence of 1,4-diazabicyclo[2.2.2]octan. This finding shows that the presence of an organic base of 1,4-diazabicyclo[2.2.2]octan is in favor of formation of the hydroxyl group. Attempts to get single crystals of other lanthanide compounds by reacting $Ln(NO_3)_3$ with H_4-DSNDA in the presence of 1,4-diazabicyclo[2.2.2]octan were unsuccessful. Compounds **2**−**8** were obtained by hydrothermal reactions of the appropriate $Ln(NO_3)_3$ with H_4-DSNDA ligand. All are 2D layered structures but belong to two structural types. In compound $[Ln(H_2\text{-}DSNDA)_{0.5}(DSNDA)_{0.5}(H_2O)_5]_n$ (Ln = La(**2**), Nd(**3**), Sm(**4**), Eu(**5**), Gd(**6**), and Dy(**7**)) each lanthanide ion is nine coordinated and surrounded by three organic ligands. While in compound $\{[Er(H\text{-}DSNDA)\cdot(H_2O)_4](H_2O)\}_n$ (**8**) the erbium ion is eight coordinated and surrounded by four organic ligands. No suitable product is

dx.doi.org/10.1021/ic2023727 | Inorg. Chem. 2012, 51, 2381−2392

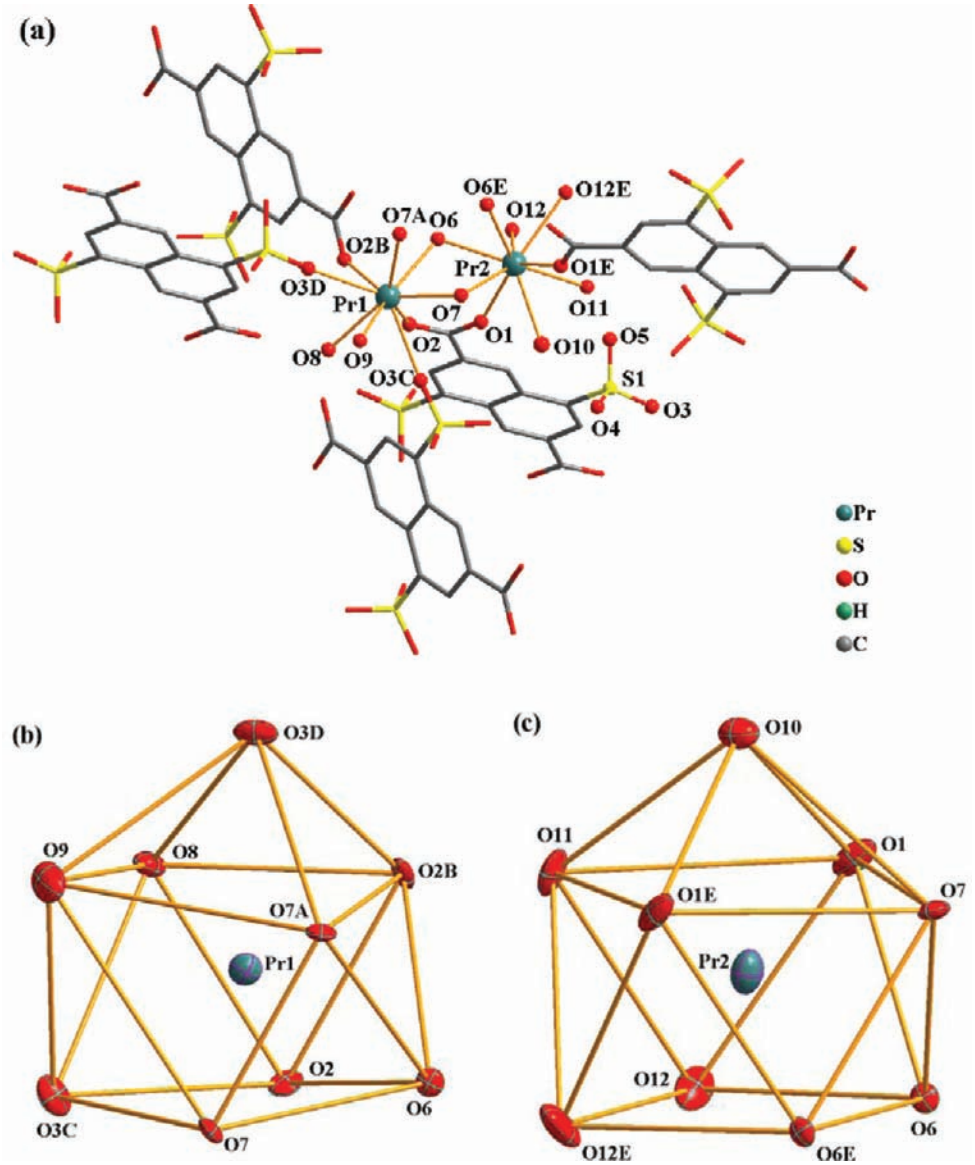

Figure 1. (a) Coordination environment of Pr(III) centers, and (b and c) coordination polyhedrons around the Pr ions in **1**.

obtained using $Tb(NO_3)_3$, $Ho(NO_3)_3$, or $Yb(NO_3)_3$ with the H_4-DSNDA ligand in similar reactions.

Crystal Structure of $\{[Pr_4(OH)_4(DSNDA)_2(H_2O)_{12}]\cdot(H_2O)_{10}\}_n$ (1). Compound **1** features a 3D framework based on the unique cubane-shaped $[Pr_4(\mu_3\text{-}OH)_4]$ cluster as a secondary building unit (SBU). As shown in Figure 1, there are two crystallographically unique Pr(III) ions in the asymmetric unit. Both are nine coordinate. The Pr1 ion is coordinated to nine oxygen atoms, three (O6, O7, and O7A) from three hydroxyl groups, two (O2 and O2B) from two carboxylate groups of the two $DSNDA^{4-}$ ligands, two (O3C and O3D) from the two sulfonate groups of the two $DSNDA^{4-}$ ligands, and two (O8 and O9) from the two water molecules (Figure 1a). The Pr2 ion is coordinated to three hydroxyl oxygen atoms (O6, O7, and O6E), two carboxylate oxygen atoms (O1 and O1E) from two the $DSNDA^{4-}$ ligands, and four water oxygen atoms (O10, O11, O12, and O12E) (Figure 1a). The coordination polyhedrons around the two Pr(III) ions can be attributed to monocapped square antiprisms with O3D and O10 at the capped positions, respectively (Figure 1b and 1c). The Pr−O bond lengths vary from 2.361(6) to 2.679(7) Å (Table S1, Supporting Information), which are comparable to those in other Pr(III) compounds.[17] As shown in Figure 2, four triply bridging μ_3-hydroxyl oxygen atoms link four Pr(III) ions to form a cubane-shaped tetranuclear $[Pr_4(\mu_3\text{-}OH)_4]$ SBU where a Pr_4 tetrahedron is embedded in the $[Pr_4(\mu_3\text{-}OH)_4]$ unit. It is to be noted that the $[Pr_4(\mu_3\text{-}OH)_4]$ cubane cluster has two crystallographically imposed mirror planes of symmetry: one mirror plane passes through Pr1, Pr1A, O6, and O6E atoms, and the other passes through Pr2, Pr2A, O7, and O7A atoms. The Pr1···Pr2, Pr1··· Pr1A, and Pr2··· Pr2A separations are 3.9216(8), 4.223(2), and 4.0848(16) Å, respectively. As depicted in Figure 2, four short edges of the Pr_4 tetrahedron is further connected by four carboxylate arms. Each $DSNDA^{4-}$ ligand locates on an inversion center and exhibits a hexadentate coordination mode with two bidentate carboxylate groups and two monodentate sulfonate groups (Scheme 2a). As shown in Figure 2, each $[Pr_4(\mu_3\text{-}OH)_4]$ cluster is surrounded by eight $DSNDA^{4-}$ ligands, which link the $[Pr_4(\mu_3\text{-}OH)_4]$ clusters to form a 3D framework with 1D rhombus-shaped channels along the crystallographic *c* direction (Figure 3) in which solvent

dx.doi.org/10.1021/ic2023727 | *Inorg. Chem.* 2012, 51, 2381−2392

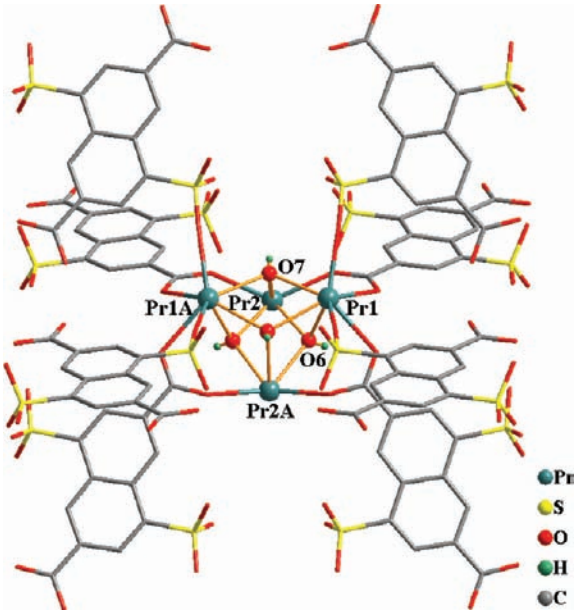

Figure 2. Tetranuclear $[Pr_4(\mu_3\text{-}OH)_4]$ SBU surrounded by eight $DSNDA^{4-}$ ligands.

Scheme 2. Observed Coordination Modes of the H_4-DSNDA Ligand

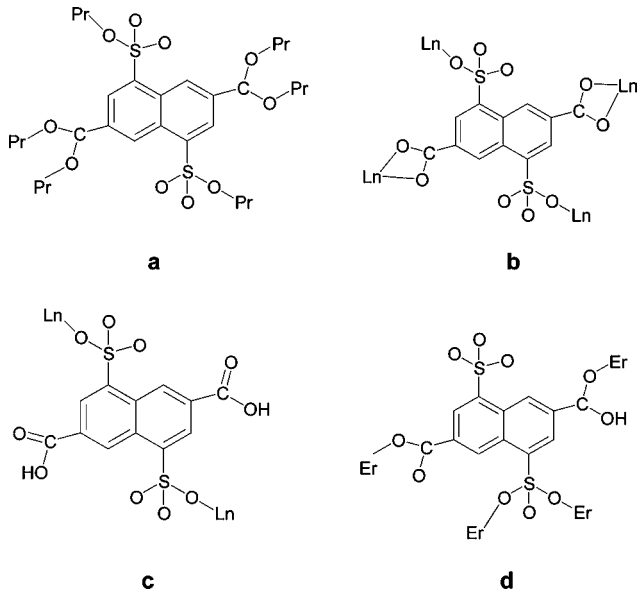

water and coordinated molecules are located. The free pore volume is 25.3% when all the water molecules are removed.

Better insight into the nature of this intricate framework can be achieved by application of a topological approach. As described above, each $[Pr_4(\mu_3\text{-}OH)_4]$ SBU is surrounded by eight $DSNDA^{4-}$ ligands and each $DSNDA^{4-}$ ligand bridges four neighboring $[Pr_4(\mu_3\text{-}OH)_4]$ SBUs. In this way, the $DSNDA^{4-}$ ligand and the $[Pr_4(\mu_3\text{-}OH)_4]$ SBU act as 4- and 8-connected nodes, respectively, in a ratio of 2:1. Therefore, structure **1** is a binodal network with 4- and 8-connected nodes. The Schäfli notation is $(4^{16}\cdot6^{12})$ for the $[Pr_4(\mu_3\text{-}OH)_4]$ node and $(4^4\cdot6^2)$ for the $DSNDA^{4-}$ node, giving the whole net symbol $(4^{16}\cdot6^{12})$-$(4^4\cdot6^2)_2$, as depicted in Figure 4. As we know, it is usually believed that the 4 and 8 connectivities would like to fall into the fluorite (CaF_2) structure of **flu**-$(4^{12}\cdot6^{12}\cdot8^4)(4^6)_2$ topology,

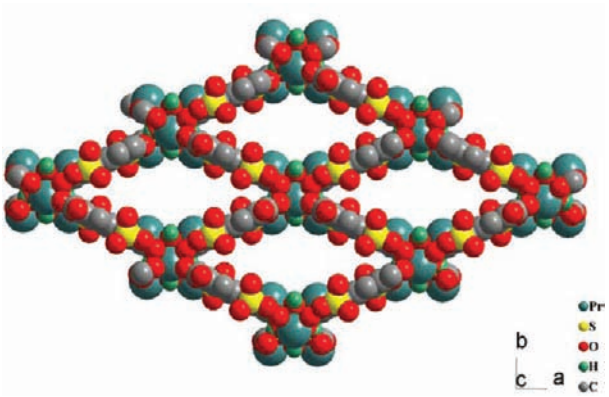

Figure 3. View of the 3D structure of **1** showing the rhombic channels (all water molecules are omitted).

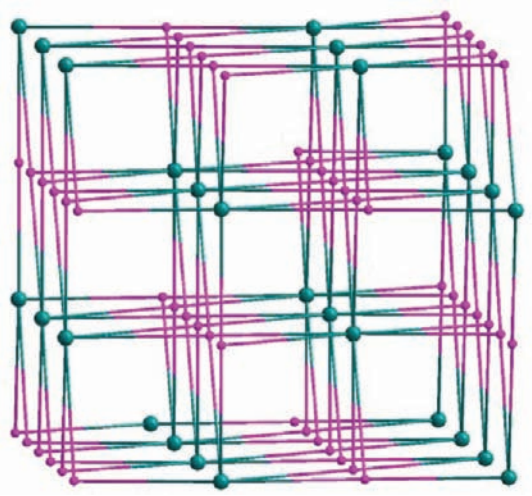

Figure 4. View of the binodal (4, 8)-connected topologic network of **1** ($[Pr_4(\mu_3\text{-}OH)_4]$ unit and $DSNDA^{4-}$ ligand represented as green and pink ball modes, respectively).

which is one of the most important and a unique topology for connecting regular cubic and tetrahedral building blocks.[18] However, structure **1** adopts an uncommon $(4^{16}\cdot6^{12})(4^4\cdot6^2)_2$ topology. To the best of our knowledge, this topology has not been observed in coordination polymers yet to date, and the finding of this unprecedented topology is useful at the basic level in the crystal engineering of coordination networks. Notice that the coordination networks of high connectivity (>6) are extremely rare because of steric constrains, especially for the fluorite topology, which requires a cubic 8-coordinated metal center (or metal cluster) and a tetrahedral 4-connected ligand.[19] Interestingly, the present net with 8-connected SBUs and 4-connected ligand is different from that of the **flu** net but related to it. If we take a careful look at the two nodes of the 3D network of **1**, their similarity and difference become apparent. As shown in Figure 4, the eight 4-connected nodes surrounding the central 8-connected node form two planes with a dihedral angle of 90°, which is same as that of the **flu** net. The 4-connected node in the **flu** net is a tetrahedral node. In the present structure, the $DSNDA^{4-}$ ligand occupies an inversion center and all the atoms of the $DSNDA^{4-}$ ligand are coplanar except for the uncoordinated sulfonate oxygen atoms (O4 and O5). Thus, the $DSNDA^{4-}$ ligand node acts as a planar 4-connected node, as depicted in Figure 4. As a result, the planar

dx.doi.org/10.1021/ic2023727 | Inorg. Chem. 2012, 51, 2381–2392

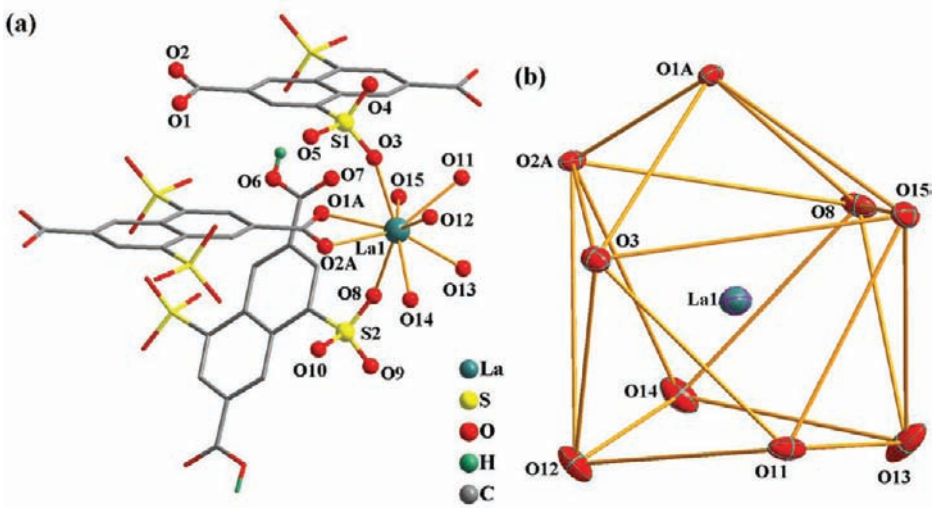

Figure 5. (a) Coordination environment of the La(III) center, and (b) coordination polyhedron around the La ion in **2**.

4-connected node is surrounded by two 6-membered and four 4-membered shortest circuits. There are six 4-membered shortest circuits around each 4-connected node in the **flu** net. As a result of these essential differences, the topology of the material changes $(4^{12}\cdot6^{12}\cdot8^4)(4^6)_2$ to $(4^{16}\cdot6^{12})(4^4\cdot6^2)_2$ topology. In addition, a related (4, 8)-connected net with $(4^{11}\cdot6^{14}\cdot8^3)$-$(4^5\cdot6)_2$ topology has been reported recently, where the tetranuclear $[Cu_4(\mu_3\text{-}OH)_2]$ SBU and the 5-sulfoisophthalate ligand can be represented by cubic and tetrahedral units, respectively.[20] However, the 8-connected node is seriously distorted from the regular cubic node due to the low symmetry of the tetranuclear $[Cu_4(\mu_3\text{-}OH)_2]$ SBU, which lead to the topological symbol being also different from that of the **flu** net.

Crystal Structure of $[Ln(H_2\text{-}DSNDA)_{0.5}(DSNDA)_{0.5}(H_2O)_5]_n$ (Ln = La(2), Nd(3), Sm(4), Eu(5), Gd(6), Dy(7)). Single-crystal X-ray analyses revealed that compounds **2**−**7** are isostructural, and the structure of La(**2**) is selected and described here representatively to illustrate their detailed structures. The asymmetric unit of compound **2** contains one La(III) ion, one-half-occupied H_2-$DSNDA^{2-}$ dianion, one-half-occupied $DSNDA^{4-}$ tetraanion, and five coordinated water molecules. It is noted that the compound contains the dianionic H_2-$DSNDA^{2-}$ and tetraanionic $DSNDA^{4-}$ ligands, both of which are centrosymmetric. As depicted in Figure 5, the La(III) ion lies on a general position and is nine coordinated with an O_9 donor set: two (O1A and O2A) from one carboxylate group of a $DSNDA^{4-}$ ligand, two (O3 and O8) from two sulfonate groups of one H_2-$DSNDA^{2-}$ ligand and one $DSNDA^{4-}$ ligand, and five from water molecules. The coordination geometry of the La(III) ion can be best described as a distorted monocapped square antiprism with O1A at the capped position (Figure 5b). The La−O distances range from 2.5104(15) to 2.5846(14) Å (Table S1, Supporting Information). The uncoordinated carboxylate groups of H_2-$DSNDA^{2-}$ ligand are protonated for charge balance, as suggested by the strong absorption at about 1700 cm^{-1} in the IR spectrum. Detailed coordination modes of the ligands are shown in Scheme 2b and 2c. The $DSNDA^{4-}$ ligand bridges four La(III) ions by two chelating carboxylate groups and two monodentate sulfonate groups, displaying a tetradentate fashion. The La(III) ions are linked by the tetraanionic $DSNDA^{4-}$ ligands along the *a* axis, forming a 1D chain, as shown in Figure 6. Adjacent chains are linked by the

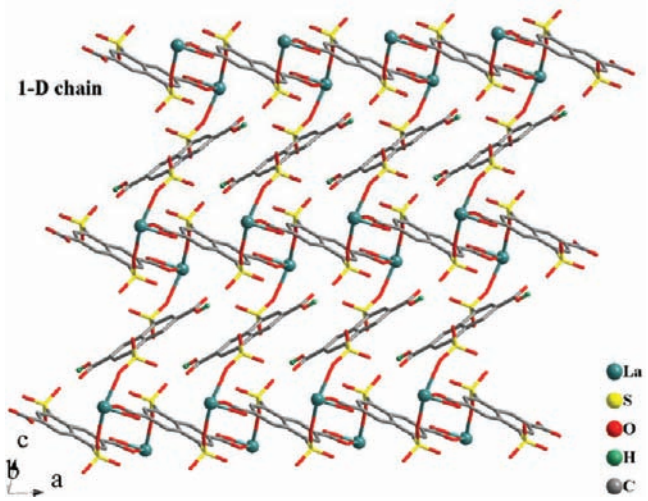

Figure 6. 2D layered structure of **2**.

bidentate H_2-$DSNDA^{2-}$ ligand with two monodentate sulfonate groups to give a 2D layer propagating along the *ac* plane (Figure 6). The 2D layer is further extended into a 3D network through extensive hydrogen bonds (Figure S1 and Table S2, Supporting Information).

Crystal Structure of $\{[Er(H\text{-}DSNDA)(H_2O)_4](H_2O)\}_n$ (8). Compound **8** features a 2D layer that is different from those of compounds **2**−**7**. There is one unique Er(III) ion in the asymmetric unit. As shown in Figure 7, the Er(III) ion located on a mirror plane is coordinated to eight oxygen atoms. The coordination sphere consists of two monodentate carboxylate oxygen atoms (O1B and O3C) from two H-$DSNDA^{3-}$ ligands and two monodentate sulfonate oxygen atoms (O7 and O7A) from the other two H-$DSNDA^{3-}$ ligands. The remaining positions are occupied by four coordinated water molecules (O9, O9A, O10, O11) (Figure 7a). The coordination environment of the Er(III) ion can be best described as a trigonal dodecahedron (Figure 7b). The H-$DSNDA^{3-}$ ligand occupies a mirror plane in which all atoms pass through the mirror plane except for two pairs of sulfonate oxygen atoms (O6 and O6D; O7 and O7D). The IR spectrum of **8** shows a sharp strong absorption at 1685 cm^{-1}, indicating that protonation of cthe arboxylate group of the H-$DSNDA^{3-}$

dx.doi.org/10.1021/ic2023727 | *Inorg. Chem.* 2012, 51, 2381−2392

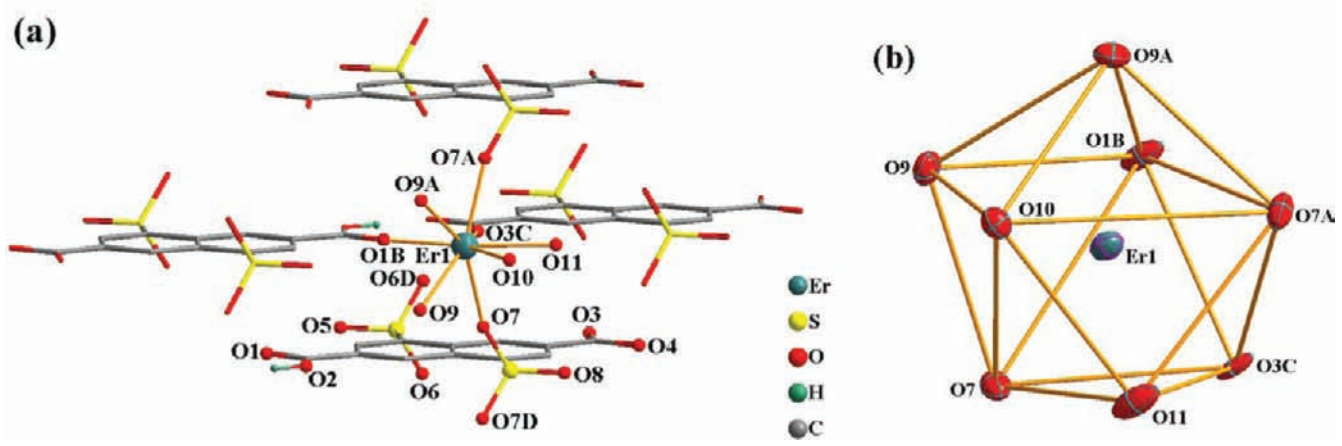

Figure 7. (a) Coordination environment of the Er(III) center, and (b) coordination polyhedron around the Er ion in **8**.

ligand exists, which is needed for charge balance. The H-DSNDA^{3-} ligand adopts a tetradentate coordination mode with two monodentate carboxylate groups and one bidentate sulfonate group (Scheme 2d). The other sulfonate group is free of coordination and engaged in hydrogen bonding with the coordinated water molecules. The Er(III) ions are linked by the H-DSNDA^{3-} ligands to produce a 2D layer propagating along the *bc* plane, as shown in Figure 8. The 2D layer has an

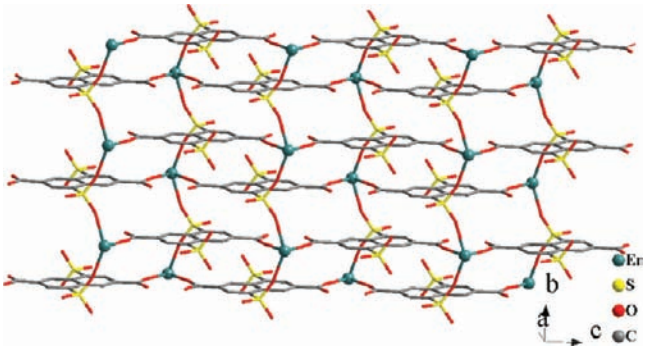

Figure 8. 2D layer of **8**.

approximate thickness of the 6.87 Å and is extended into a 3D framework through the interlayered hydrogen bonds between coordinated water molecules and sulfonate oxygen atoms (Figure S2 and Table S2, Supporting Information).

FT-IR Spectra and Thermogravimetric Analysis. For the H_4-DSNDA ligand, four characteristic absorption bands at 1243, 1194, 1112, and 1048 cm^{-1} in the IR spectrum are clearly observed, which are attributable to the O═S═O stretching vibrations of the $-SO_3H$ groups. The absorption band at 615 cm^{-1} assigned to the C−S stretching vibrations was also detected. The infrared spectra of compounds **1**−**8** show similar main characteristic peaks since they all contain the same organic ligand. The IR spectra of these compounds exhibit broad absorption bands in the range 3500−3410 cm^{-1} due to the presence of water molecules in the structures. The strong bands at 1360−1650 cm^{-1} for all compounds are characteristic of the carboxylate groups. The strong absorption at about 1690 cm^{-1} for compounds **2**−**8** indicates the existence of the protonated carboxylate groups of the organic ligand. The absorptions in the region 1000−1240 cm^{-1} for all compounds are typical of the sulfonate group. The sharp absorptions at about 605 cm^{-1} for all compounds can be assigned to the C−S stretching vibrations.

To examine the thermal stability of these compounds and their structural variation as a function of temperature thermogravimetric analysis (TGA) was performed on crystalline samples of these materials (Figure S3, Supporting Information). The TGA trace for compound Pr(**1**) displays a small gradual weight loss starting at 40 °C, and then a sharp continual weight loss occurred at 100 °C. The total observed weight loss between 40 and 155 °C is 16.38%, which is attributed to release of all 10 solvent water molecules and 6 coordinated water molecules (theoretical 16.25%) and then a gradual mass loss of 5.82% between 170 and 310 °C, which is attributed to removal of the remaining six-coordinated water molecules (theoretical 6.09%). The main framework of the compound starts to decompose at 380 °C. Compounds **2**−**7** will show similar thermal behavior since they are isostructural. Therefore, only one representative La(**2**) compound is discussed. Compound La(**2**) is stable up to 110 °C and then exhibits two main steps of weight losses. The first step (110−180 °C) corresponds to release of four coordinated water molecules (weight loss = measured 12.19%; theoretical 11.96%). The second weight loss in the temperature range 270−310 °C corresponds to loss of the remaining coordinated water molecule (weight loss = measured 3.13%; theoretical 2.99%). Decomposition of the framework occurs at 400 °C. Compound Er(**8**) is not stable and displays a rapid continual mass loss of 14.71% between 40 and 265 °C, which is attributed to release of all water molecules (theoretical 14.27%). Collapse of the framework occurs at 400 °C.

Photoluminescent Properties. Considering the characteristic luminescent properties of Eu(III)-containing compounds in the visible region, the solid-state luminescent spectra of compound Eu(**5**) were measured at room temperature. As shown in Figure 9, free H_4-DSNDA ligand displays a photoluminescent emission at 408 nm upon excitation at 350 nm. The photoluminescence of the free ligand has been assigned as originating from the intraligand (IL) $\pi^*-\pi$ electron transitions. The excitation spectrum of compound Eu(**5**) exhibits a broad excitation band between 250 and 500 nm, as depicted in Figure 10. The broad excitation band could be primarily assigned to the $\pi^*-\pi$ electron transitions of the organic ligand. In the excitation spectrum it is also possible to discern the $^7F_0 \rightarrow {}^5L_6$ (396 nm) and $^7F_0 \rightarrow {}^5D_2$ (465 nm) intra-4f^6 transitions of the Eu(III) ion (Figure 10),[21] although the

dx.doi.org/10.1021/ic2023727 | *Inorg. Chem.* 2012, 51, 2381−2392

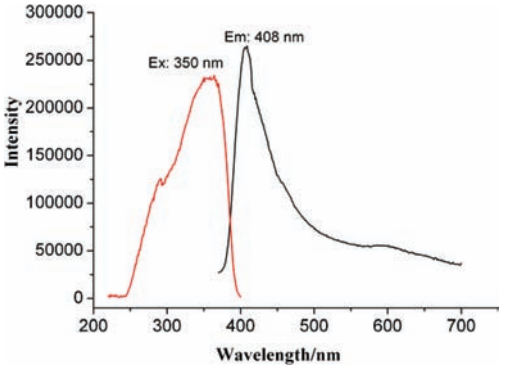

Figure 9. Solid-state excitation and emission spectra of the H_4-DSNDA ligand at room temperature.

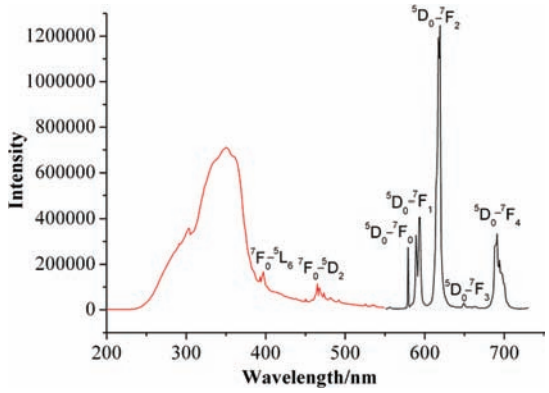

Figure 10. Room-temperature excitation (red) with emission monitored at approximately 618 nm, and emission (black) spectra for compound Eu(**5**) (λ_{ex} = 350 nm) in the solid state.

intensities of the peaks were very weak. The broad band overlaps intra-4f^6 lines. The absence or negligible intensity of the intra-4f^6 transitions in the excitation spectrum indicates that the Eu(III) ions are mainly excited via an effective sensitized process involving the organic ligand excited states, rather than by direct excitation of the Eu(III) ion. Compound Eu(**5**) exhibits a very strong and characteristic emission spectrum of the Eu(III) ion upon excitation at 350 nm (Figure 10). The emission bands occurring at 579, 593, 617, 650, and 694 nm can be assigned to $^5D_0 \rightarrow {}^7F_J$ (J = 0 1, 2, 3, and 4) transitions. It is well known that the $^5D_0 \rightarrow {}^7F_2$ and $^5D_0 \rightarrow {}^7F_1$ transitions of the Eu(III) ion are electric-dipole (ED) and magnetic-dipole (MD), respectively. The former is extremely sensitive to site symmetry, while the latter whose emission intensity is mainly dependent on the crystal field around the Eu(III) ion is insensitive to site symmetry. The intensity of the $^5D_0 \rightarrow {}^7F_2$ transition is about 3.5 times stronger than that of the $^5D_0 \rightarrow {}^7F_1$ transition, indicating that the coordination environment of the Eu(III) ion is asymmetric,[22] in agreement with single-crystal X-ray analysis. Moreover, the $^5D_0 \rightarrow {}^7F_0$ transition induced by crystal-field J mixing is also observed in the emission spectrum of compound Eu(**5**). According to the electric-dipole selection rule, the $^5D_0 \rightarrow {}^7F_0$ emission is only allowed for C_s, C_n, and C_{nv} (n = 1, 2, 3, 4, 6) site symmetry.[23,24] As described above, compound Eu(**5**) crystallizes from the triclinic crystal system and the Eu(III) ion lies on a general position. Thus, the actual site symmetry of the Eu(III) ion belongs to the lowest symmetry of C_1. Thus, it is not unreasonable to observe the $^5D_0 \rightarrow {}^7F_0$ transition in the emission spectrum of compound Eu(**5**).

The $^5D_0$ emission decay curve was monitored within the $^5D_0 \rightarrow {}^7F_2$ transition under the excitation wavelength (Figure S4, Supporting Information). However, the decay curve cannot fit into the single-exponential function like some reported Eu(III) coordination compounds[25,26] but can be well fit into a double-exponential function as $I = A + B_1 \exp(-t/\tau_1) + B_2 \exp(-t/\tau_2)$ (where τ_1 and τ_2 are the fast and slow components of the luminescent lifetimes and A, B_1, and B_2 are the fitting parameters). The lifetimes for $^5D_0 \rightarrow {}^7F_2$ of the Eu(III) ion were calculated to be τ_1 = 0.153 ms and τ_2 = 0.474 ms. The average lifetime of $^5D_0 \rightarrow {}^7F_2$ for the Eu(III) ion, defined as $\langle\tau\rangle = (B_1\tau_1^2 + B_2\tau_2^2)/(B_1\tau_1 + B_2\tau_2)$,[27] can be determined to be 0.171 ms (fitting parameters B_1 = 2066 and B_2 = 40.28). The double-exponential decay behavior of the activator is often observed when the excitation energy is transferred from the donor,[28] which indicates efficient energy transfer occurs from the organic ligand to the Eu(III) ion.

Magnetic Properties. The dc magnetic susceptibilities for all compounds except for the La(**2**) compound were measured in an applied dc field of 1 or 0.1 kOe. For these compounds the observed paramagnetism arises uniquely from the 4f Ln(III) ions. The temperature dependence of the magnetic susceptibility studies for compound Pr(**1**) has been performed in the temperature range 2−300 K. The plot of $\chi_M T$ versus T, where χ_M is the molar magnetic susceptibility per Pr_4 unit, is shown in Figure 11. At 300 K, the $\chi_M T$ value of 4.81 cm^3 K mol^{-1} is lower

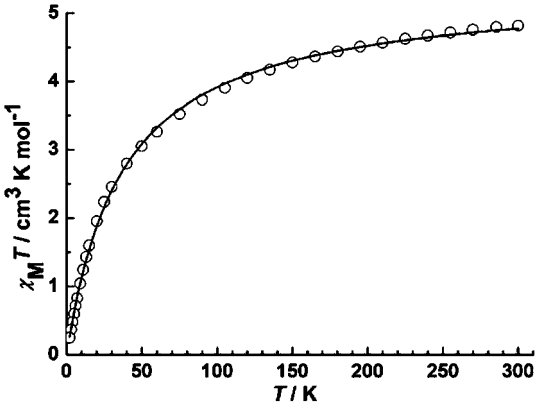

Figure 11. Temperature dependence of the $\chi_M T$ product at 1 kOe for Pr (**1**). Solid line is the best fit obtained with the model as described in the text.

than the expected value of 6.4 cm^3 K mol^{-1} for four uncoupled Pr(III) ions (S = 1, L = 5, $^3H_4$, g = 4/5). $\chi_M T$ gradually decreases to reach 0.25 cm^3 K mol^{-1} at 2 K, which is probably the result of a combination of the exchange interaction between the Pr(III) ions and the progressive depopulation of excited Stark sublevels. There is no available expression to determine the magnetic susceptibilities of such 3D system with large anisotropy. To obtain a rough quantitative estimation of the magnetic interaction between Pr(III) ions, as a preliminary treatment, we assumed that owing to the ligand field effects the Pr(III) ion may exhibit a splitting of m_j energy levels ($\hat{H} = \Delta\hat{J}_Z^2$), resulting in the magnetic susceptibility equation below previously reported by McPherson and co-workers.[29] Thus, χ_{Pr} can be described as eq 1.

$$\chi_{Pr} = \frac{Ng^2\beta^2}{kT}\frac{[2e^{(-\Delta/kT)} + 8e^{(-4\Delta/kT)} + 18e^{(-9\Delta/kT)} + 32e^{(-16\Delta/kT)}]}{[1 + 2e^{(-\Delta/kT)} + 2e^{(-4\Delta/kT)} + 2e^{(-9\Delta/kT)} + 2e^{(-16\Delta/kT)}]} \quad (1)$$

dx.doi.org/10.1021/ic2023727 | Inorg. Chem. 2012, 51, 2381−2392

$$\chi = \frac{\chi_{Ln}}{1 - (2zJ'/Ng^2\beta^2)\chi_{Ln}} \quad (2)$$

In this expression Δ is the zero-field splitting parameter and N, g, β, and k have their usual meanings. Using the above equation and considering the molecular field approximation with zJ' as the total exchange parameter between Pr(III) ions we can fit our experimental data with eq 2. The best fitting of the susceptibility data in the temperature range 2−300 K gives $zJ' = -1.79$ cm^{-1}, $\Delta = 0.33$ cm^{-1}, $g = 0.73$, and $R^2 = 0.99929$. The negative value of zJ' indicates that an overall antiferromagnetic interaction between Pr(III) ions is operative.

The plot of $\chi_M T$ versus T for compound Nd(**3**) in the temperature range 2−300 K, where χ_M is the molar magnetic susceptibility per Nd(III) unit, is shown in Figure 12. At 300 K,

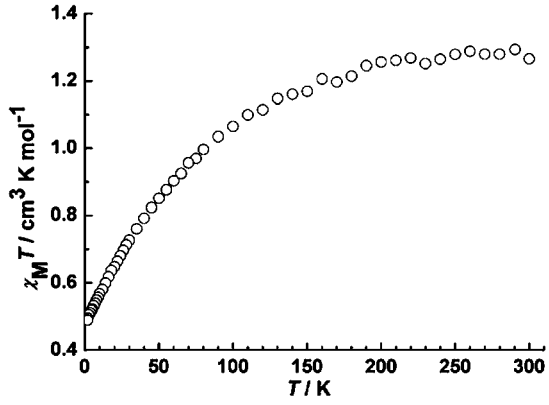

Figure 12. Temperature dependence of the $\chi_M T$ product at 0.1 kOe for Nd(**3**).

the $\chi_M T$ value of 1.26 cm^3 K cm^{-1} is lower than the expected value of 1.64 cm^3 K cm^{-1} for one insulated Nd(III) ion ($S = 3/2$, $L = 6$, $^4I_{9/2}$, $g = 8/11$). $\chi_M T$ gradually decreases to reach 0.49 cm^3 K cm^{-1} at 2 K, which is probably the result of a combination of the exchange interaction between the Nd(III) ions and the progressive depopulation of excited Stark sublevels.[30] There is no available expression to determine the magnetic susceptibilities of such 2D system with large anisotropy. To obtain a rough quantitative estimation of the magnetic interaction between Nd(III) ions, as a preliminary treatment, we assumed that owing to the ligand field effects, the Nd(III) ion may exhibit a splitting of m_j energy levels ($\hat{H} = \Delta\hat{J}_Z^2$), resulting in a magnetic susceptibility equation in which χ_{Nd} can be described as eq 3.

$$\chi_{Nd} = \frac{Ng^2\beta^2}{4kT}\frac{[81e^{(-81\Delta/4kT)} + 49e^{(-49\Delta/4kT)} + 25e^{(-25\Delta/4kT)} + 9e^{(-9\Delta/4kT)} + e^{(-\Delta/4kT)}]}{[e^{(-81\Delta/4kT)} + e^{(-49\Delta/4kT)} + e^{(-25\Delta/4kT)} + e^{(-9\Delta/4kT)} + e^{(-\Delta/4kT)}]} \quad (3)$$

Unfortunately, however, combining eqs 2 and 3 we cannot gain a satisfied result. As is well known, due to the presence of thermally populated excited state and large magnetic anisotropy for most lanthanide ions, the fitting of the susceptibility curve is difficult. The low-temperature magnetization measurement as a function of the field for Nd(**3**) is represented in Figure S5, Supporting Information; the magnetization increases rapidly at low field before a gradual linear increase. The magnetization does not saturate but reaches 1.19 μ_B at 1.8 K in a field of 7 T. This value is much lower than the expected saturation value of 3.27 μ_B, which is indicative of antiferromagnetic coupling occurring between Nd(III) ions, in combination with considerable spin−orbit effects.

Magnetic susceptibility measurements of Sm(**4**) and Eu(**5**) were performed in an applied magnetic field of 0.1 kOe in the 2−300 K range. They are shown in Figure 13 for Sm(**4**) and

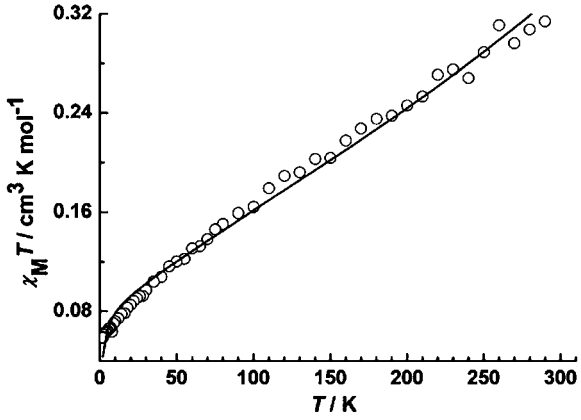

Figure 13. Temperature dependence of the $\chi_M T$ product at 0.1 kOe for Sm(**4**). Solid line is the best fit obtained with the model as described in the text.

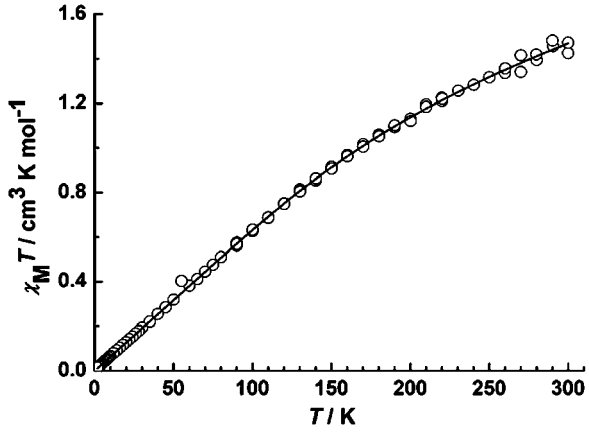

Figure 14. Temperature dependence of the $\chi_M T$ product at 0.1 kOe for Eu(**5**). Solid line is the best fit obtained with the model as described in the text.

Figure 14 for Eu(**5**). The $\chi_M T$ values of 0.31 (Sm(**4**)) and 1.42 cm^3 K mol^{-1} (Eu(**5**)) are much higher than the theoretical values of 0.088 and 0 cm^3 K mol^{-1} for one isolated Sm(III) ($S = 5/2$, $L = 5/2$,$^6H_{5/2}$, $g = 2/7$) and Eu(III) ions ($S = 3$, $L = 3$, $^7F_0$, $g = 5$) in the ground state, respectively, because not only the ground state of these two metal ions but also the first ($^6H_{7/2}$ for Sm(III) and $^7F_1$ for Eu(III)) and even higher exited states can be populated at room temperature.[31] The rapid decrease in the $\chi_M T$ values for both compounds upon lowering the temperature are mainly due to thermal depopulation of the excited levels. The typical nonmagnetic ground state $^7F_0$ is observed at low temperatures for Eu(**5**) as suggested by the $\chi_M T$ value of 0.013 at 1.8 K.[31] The molar magnetic susceptibilities can be expressed by eqs 4 and 5, respectively, which take into account both the ground state and the exited states (^6H_J, $J = 7/2$, 9/2, 11/2, 13/2, 15/2 for Sm(**4**); ^7F_J, $J = 1$, 2, 3, ..., 6 for Eu(**5**)).[32]

dx.doi.org/10.1021/ic2023727 | Inorg. Chem. 2012, 51, 2381−2392

In these two expressions $x = \lambda/kT$ (λ is the spin−orbit coupling parameter), the zJ' parameter based on the molecular field approximation

$$\chi_{Sm} = \frac{N\beta^2}{3kTx}\frac{[2.143x + 7.347 + (42.92x + 1.641)e^{-7x/2} + (283.7x - 0.6571)e^{-9x} + (620.6x - 1.94)e^{-35x/2} + (1122x - 2.835)e^{-30x} + (1813x - 3.556)e^{-55x/2}]}{[3 + 4e^{-7x/2} + 5e^{-9x} + 6e^{-27x/2} + 7e^{-20x} + 8e^{-35x/2}]} \quad (4)$$

$$\chi_{Eu} = \frac{N\beta^2}{3kTx}\frac{[24 + (13.5x - 1.5)e^{-x} + (67.5x - 2.5)e^{-3x} + (189x - 3.5)e^{-6x} + (405x - 4.5)e^{-10x} + (742.5x - 5.5)e^{-15x} + (1228.5x - 6.5)e^{-21x}]}{[1 + 3e^{-x} + 5e^{-3x} + 7e^{-6x} + 9e^{-10x} + 11e^{-15x} + 13e^{-21x}]} \quad (5)$$

The best fit gives $g = 0.98$, $\lambda = 254$ cm^{-1}, $zJ' = -2.63$ cm^{-1}, and $R^2 = 0.99148$ for Sm(**4**) in the range 2−300 K. For Eu(**5**) the parameters are $g = 1.14$, $\lambda = 323$ cm^{-1}, $zJ' = -6.58$ cm^{-1}, and $R^2 = 0.99935$ in the range 2−300 K. The negative zJ' values are indicative of the antiferromagnetic interaction between the Ln(III) ions in both compounds. The field dependence of the magnetization at 1.8 K for Sm(**4**) reveals a gradual linear increase of the magnetization (Figure S5, Supporting Information). The magnetization does not saturate but reaches 0.26 μ_B in a field of 7 T, which is much lower than the expected saturation value of 0.84 μ_B for each Sm(III) ion.

The temperature dependence of the magnetic susceptibility of compound Gd(**6**) was determined in the 2−300 K temperature range. The result is represented in Figure 15 as

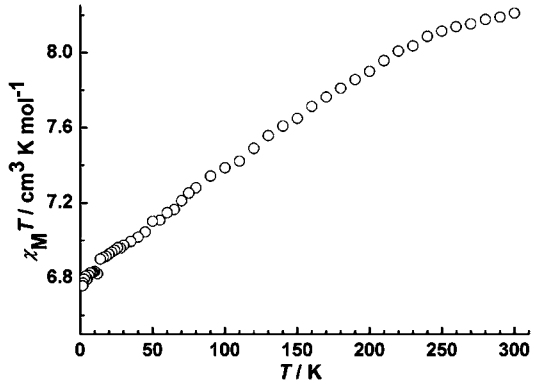

Figure 15. Temperature dependence of the $\chi_M T$ product at 0.1 kOe for Gd(**6**).

a $\chi_M T$ versus T curve (χ_M being the molar paramagnetic susceptibility per Gd(III)). At 300 K, $\chi_M T$ is 8.21 cm^3 K cm^{-1}, which is higher than the expected corresponding value of 7.87 cm^3 K cm^{-1} for one Gd(III) ($S = 7/2$, $L = 0$, $^8S_{7/2}$, $g = 2.0$). $\chi_M T$ gradually decreases to 6.75 cm^3 K cm^{-1} at 2 K. The decrease of $\chi_M T$ when lowering the temperature indicates clearly the presence of an antiferromagnetic interaction between the Gd(III) ions. It is well known that Gd(III) has a $^8S_{7/2}$ ground state without first-order orbital momentum. The magnetic susceptibility is almost isotropic and follows the Curie−Weiss law $\chi = C/(T - \theta)$. A fit of the Curie−Weiss law (Figure S6, Supporting Information) between 2 and 90 K yields $C = 7.28$ cm^3 K cm^{-1} and $\theta = -0.73$ K, further confirming the possibility of weak antiferromagnetic exchange. The field dependence of the magnetization of Gd(**6**) was collected at low temperature as shown in Figure S7, Supporting Information. The magnetization eventually reaches a value of 7.85 μ_B at 1.8 K and 7 T with near saturation.

The result of the magnetic susceptibility of compound Dy(**7**) in the 2.5−300 K temperature range is represented in Figure 16 as a $\chi_M T$ versus T curve. At 300 K, the $\chi_M T$ value is 14.18 cm^3 K cm^{-1}, which is the same as the expected value of 14.17 cm^3 K cm^{-1} for one magnetically isolated Dy(III) ($S = 5/2$, $L = 5$, $^6H_{15/2}$, $g = 4/3$) ion. Upon cooling, the $\chi_M T$ product gradually

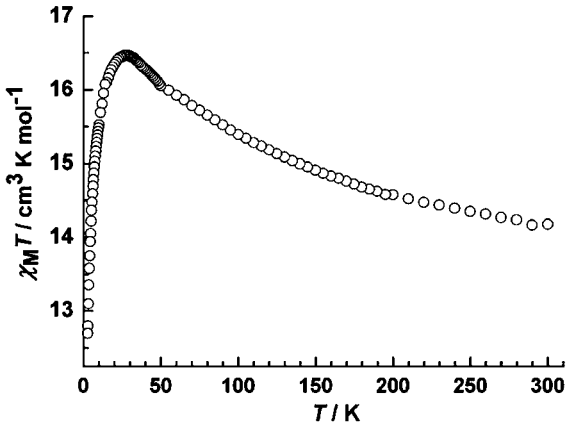

Figure 16. Temperature dependence of the $\chi_M T$ product at 1 kOe for Dy(**7**).

rises to reach a maximum value of 16.47 cm^3 K cm^{-1} at 27 K, below which the $\chi_M T$ product decreases sharply to reach a value of 12.69 cm^3 K cm^{-1} at 2.5 K. This behavior is characteristic of a system with ferromagnetic interactions. The decrease of $\chi_M T$ at low temperature is likely due to a combination of depopulation of excited Stark sublevels, large magnetic anisotropy, and intermolecular magnetic coupling. The large spin S and magnetic anisotropy D values intrinsic to the Dy(III) ion make its compounds attractive for design of single-molecule magnets, which is a hot topic of the single-molecule magnet community very recently.[33] To examine the spin dynamics the temperature dependencies of the alternating-current (ac) magnetic susceptibility for compound Dy(**7**) were collected at zero direct-current (dc) field with an ac field of 3 Oe with oscillating frequencies, given in Figure S8, Supporting Information, as plots of χ' and χ'' versus T. However, no imaginary component of the ac susceptibility χ'' was observed, which clearly excludes an SMM behavior for compound Dy(**7**) above 2.5 K.

The thermal variation of the $\chi_M T$ product for Er(**8**) is shown in Figure 17. At 300 K, $\chi_M T$ is equal to 11.80 cm^3 K cm^{-1},

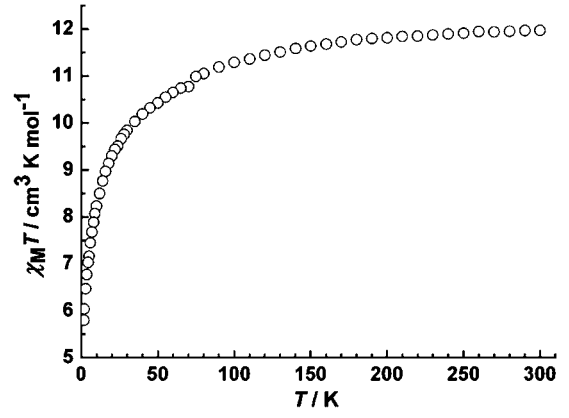

Figure 17. Temperature dependence of the $\chi_M T$ product at 0.1 kOe for Er (**8**).

which is the value expected (11.48 cm^3 K cm^{-1}) for one Er(III) ion ($S = 3/2$, $L = 6$, $^4I_{15/2}$, g = 6/5). On lowering the temperature $\chi_M T$ gradually decreases to 10.44 cm^3 K cm^{-1} at 50 K, probably the result of mainly thermal depopulation of the Er(III) excited states (Stark sublevels of the $^4I_{15/2}$ state). Below

dx.doi.org/10.1021/ic2023727 | Inorg. Chem. 2012, 51, 2381−2392

50 K, $\chi_M T$ decreases down to 5.80 cm^3 K cm^{-1} at 2 K. The decrease of $\chi_M T$ between 50 and 2 K is associated with antiferromagnetic intramolecular exchanges. The field dependence of the magnetization of Er(**8**) was collected at low temperature as shown in Figure S7, Supporting Information. Magnetization eventually reaches a value of 6.10 μ_B at 1.8 K and 7 T without clear saturation.

CONCLUSIONS

A 4,8-disulfonyl-2,6-naphthalenedicarboxylic acid (H_4-DSNDA) ligand and a series of lanthanide coordination polymers based on the H_4-DSNDA ligand have been synthesized and characterized. Compound **1** is a 3D framework with $(4^{16}\cdot6^{12})(4^4\cdot6^2)_2$ topology featuring the unique cubane-shaped $[Pr_4(\mu_3\text{-}OH)_4]$ cluster. Compounds **2**−**7** are 2D layered structures. Compound **8** has a 2D layer different from those of compounds **2**−**7**. Compound Eu(**5**) shows the characteristic red luminescence, the emission spectrum being in good agreement with the crystal structure. Finally, the magnetic behavior of the compounds is discussed in detail.

ASSOCIATED CONTENT

Supporting Information

X-ray structure data in CIF format, table of bond lengths and angles, table of hydrogen bonds, 3D hydrogen-bonded structures, TG curves, luminescence decay curve of compound Eu(**5**), *M* vs *H*/*T* magnetic data, and ac magnetic susceptibilities of compound Dy(**7**). This material is available free of charge via the Internet at http://pubs.acs.org.

AUTHOR INFORMATION

Corresponding Author

*E-mail: qyliuchem@hotmail.com (Q.-Y.L.); tang@ciac.jl.cn (J.T.).

Notes

The authors declare no competing financial interest.

ACKNOWLEDGMENTS

This work was supported by the NNSF of China (Grants 20901033 and 21101081), the Scientific Research Foundation for the Returned Overseas Chinese Scholars (State Education Ministry), the Provincial NSF of Jiangxi (2009GZH0056), and the Project of Education Department of Jiangxi Province (GJJ10016 and GJJ11381).

REFERENCES

(1) (a) Moulton, B.; Zaworotko, M. J. *Chem. Rev.* **2001**, *101*, 1629. (b) Kitagawa, S.; Kitaura, R.; Noro, S. *Angew. Chem., Int. Ed.* **2004**, *43*, 2334. (c) Eddaoudi, M.; Moler, D. B.; Li, H. L.; Chen, B. L.; Reineke, T. M.; O'Keeffe, M.; Yaghi, O. M. *Acc. Chem. Res.* **2001**, *34*, 319. (d) Wu, C.-D.; Lin, W.-B. *Angew. Chem., Int. Ed.* **2005**, *44*, 1958.

(2) (a) Maji, T. K.; Mostafa, G.; Chang, H.-C.; Kitagawa, S. *Chem. Commun.* **2005**, 2436. (b) Shiga, T.; Ito, N.; Hidaka, A.; Ohkawa, H.; Kitagawa, S.; Ohba, M. *Inorg. Chem.* **2007**, *46*, 3492. (c) Thirumurugan, A.; Natarajan, S. *Dalton Trans.* **2004**, 2923. (d) Long, D. L.; Blake, A. J.; Champness, N. R.; Wilson, C.; Schröder, M. *Angew. Chem., Int. Ed.* **2001**, *40*, 2443. (e) Pan, L.; Zheng, N. W.; Wu, Y. G.; Nan, S.; Yang, R. Y.; Huang, X. Y.; Li, J. *Inorg. Chem.* **2001**, *40*, 828. (f) Sun, Y.-Q.; Zhang, J.; Yang, G.-Y. *Chem. Commun.* **2006**, 1947. (g) Benelli, C.; Gatteschi, D. *Chem. Rev.* **2002**, *102*, 2369. (h) Cañadillas-Delgado, L.; Martín, T.; Fabelo, O.; Pasán, J.; Delgado, F. S.; Lloret, F.; Julve, M.; Ruiz-Pérez, C. *Chem.—Eur. J* **2010**, *16*, 4037.

(3) (a) Serre, C.; Férey, G. *J. Mater. Chem.* **2002**, *12*, 3053. (b) Serpaggi, F.; Férey, G. *J. Mater. Chem.* **1998**, *8*, 2749. (c) Yang, A.-H.; Gao, H.-L.; Cui, J.-Z.; Zhao, B. *CrystEngComm* **2011**, *13*, 1870. (d) Henry, N.; Costenoble, S.; Lagrenée, M.; Loiseau, T.; Abraham, F. *CrystEngComm* **2011**, *13*, 251. (e) Cai, B.; Yang, P.; Dai, J.-W.; Wu, J.-Z. *CrystEngComm* **2011**, *13*, 985.

(4) (a) Jiang, H.-L.; Tsumori, N.; Xu, Q. *Inorg. Chem.* **2010**, *49*, 10001. (b) Reineke, T. M.; Eddaoudi, M.; Fehr, M.; Kelley, D.; Yaghi, O. M. *J. Am. Chem. Soc.* **1999**, *121*, 1651. (c) Liu, T.-F.; Zhang, W. J.; Sun, W.-H.; Cao, R. *Inorg. Chem.* **2011**, *50*, 5242. (d) Ma, B.-Q.; Zhang, D.-S.; Gao, S.; Jin, T.-Z.; Yan, C.-H.; Xu, G.-X. *Angew. Chem., Int. Ed.* **2000**, *39*, 3644.

(5) (a) Côté, A. P.; Shimizu, G. K. H. *Coord. Chem. Rev.* **2003**, *245*, 49. (b) Shimizu, G. K. H.; Vaidhyanathan, R.; Taylor, J. M. *Chem. Soc. Rev.* **2009**, *38*, 1430.

(6) (a) Xiao, B.; Byrne, P. J.; Wheatley, P. S.; Wragg, D. S.; Zhao, X.; Fletcher, A. J.; Thomas, K. M.; Peters, L.; Evans, J. S. O.; Warren, J. E.; Zhou, W.; Morris, R. E. *Nat. Chem.* **2009**, *1*, 289. (b) Hurd, J. A.; Vaidhyanathan, R.; Thangadurai, V.; Ratcliffe, C. I.; Moudrakovsk, I. L.; Shimizu, G. K. H. *Nat. Chem.* **2009**, *1*, 705.

(7) (a) Dalrymple, S. A.; Shimizu, G. K. H. *J. Am. Chem. Soc.* **2007**, *129*, 12114. (b) Forbes, T. Z.; Sevov, S. C. *Inorg. Chem.* **2009**, *48*, 6873. (c) Cai, J. W. *Coord. Chem. Rev.* **2004**, *248*, 1061. (c) Videnova-Adrabinska, V. *Coord. Chem. Rev.* **2007**, *251*, 1987.

(8) (a) Liu, Q.-Y.; Wang, Y.-L.; Xu, L. *Eur. J. Inorg. Chem.* **2006**, 4843. (b) Liu, Q.-Y.; Wang, Y.-L.; Shan, Z.-M.; Cao, R.; Jiang, Y.-L.; Wang, Z.-J.; Yang, E.-L. *Inorg. Chem.* **2010**, *49*, 8191. (c) Shan, Z.-M.; Wang, Y.-L.; Liu, Q.-Y.; Zhang, N.; Yang, E.-L.; Wei, J.-J. *Inorg. Chim. Acta* **2010**, *363*, 2269. (d) Liu, Q.-Y.; Wang, Y.-L.; Zhang, N.; Jiang, Y.-L.; Wei, J.-J.; Luo, F. *Cryst. Growth Des.* **2011**, *11*, 3717.

(9) (a) Kulynych, A. D.; Shimizu, G. K. H. *CrystEngComm* **2002**, *4*, 102. (b) Sun, D. F.; Cao, R.; Sun, Y. Q.; Bi, W. H.; Yuan, D. Q.; Shi, Q.; Li, X. *Chem. Commun.* **2003**, 1528. (c) Sun, Z.-M.; Mao, J.-G.; Sun, Y.-Q.; Zeng, H.-Y.; Clearfield, A. *Inorg. Chem.* **2004**, *43*, 336.

(10) Horike, S.; Matsuda, R.; Tanaka, D.; Mizuno, M.; Endo, K.; Kitagawa, S. *J. Am. Chem. Soc.* **2006**, *128*, 4222.

(11) (a) Miao, X.-H.; Zhu, L.-G. *CrystEngComm* **2009**, *11*, 2500. (b) Prochniak, G.; Videnova-Adrabinska, V.; Daszkiewicz, M.; Pietraszko, A. *J. Mol. Struct.* **2008**, *178*, 891.

(12) (a) Yuan, R.-X.; Xiong, R.-G.; Xie, Y.-R.; You, X.-Z.; Peng, S.-M.; Lee, G.-H. *Inorg. Chem. Commun.* **2001**, *4*, 384. (b) Li, X.; Li, Y.-Q.; Wu, X.-S. *Inorg. Chem. Commun.* **2008**, *11*, 774. (c) Zhang, L.-P.; Zhu, L.-G. *CrystEngComm* **2006**, *8*, 815.

(13) Papadaki, I.; Malliakas, C. D.; Bakas, T.; Trikalitis, P. N. *Inorg. Chem.* **2009**, *48*, 9968.

(14) Qing, S.; Huang, W.; Yan, D. *React. Funct. Polym.* **2006**, *66*, 219.

(15) Sheldrick, G. M. *SADABS*; University of Göttingen: Göttingen, Germany, 1995.

(16) Sheldrick, G. M. *Acta Crystallogr.* **2008**, *A64*, 112.

(17) (a) Cepeda, J.; Balda, R.; Beobide, G.; Castillo, O.; Fernández, J.; Luque, A.; Pérez-Yáñez, S.; Román, P.; Vallejo-Sánchez, D. *Inorg. Chem.* **2011**, *50*, 8437. (b) Liu, Q.-Y.; Xu, L. *Eur. J. Inorg. Chem.* **2005**, 3458.

(18) O'Keeffe, M.; Eddaoudi, M.; Li, H.-L.; Reineke, T.; Yaghi, O. M. *J. Solid State Chem.* **2000**, *152*, 3.

(19) Chun, H.; Kim, D.; Dybtsev, D. N.; Kim, K. *Angew. Chem., Int. Ed.* **2004**, *43*, 971.

(20) Liu, Q.-Y.; Yuan, D.-Q.; Xu, L. *Cryst. Growth Des.* **2007**, *7*, 1832.

(21) Albin, M.; Wright, R. R.; Horrocks, W. D. *Inorg. Chem.* **1985**, *24*, 4591.

(22) Kirby, A. F.; Foster, D.; Richardson, F. S. *Chem. Phys. Lett.* **1983**, *95*, 507.

(23) Nogami, M.; Abe, Y. J. *Non-Cryst. Solids* **1996**, *197*, 73.

(24) Blasse, G.; Bril, A. *Philips Res. Rep* **1966**, *2*, 368.

(25) Li, X. F.; Liu, T. F.; Lin, Q. P.; Cao, R. *Cryst. Growth Des.* **2010**, *10*, 608.

(26) Yan, X. H.; Cai, Z. C.; Yi, C. L.; Liu, W. S.; Tan, M. Y.; Tang, Y. *Inorg. Chem.* **2011**, *50*, 2346.

(27) (a) Fujii, T.; Kodaira, K.; Kawauchi, O.; Tanaka, N.; Yamashita, H.; Anpo, M. *J. Phys. Chem. B* **1997**, *101*, 10631. (b) Murakami, S.;

Herren, M.; Rau, D.; Morita, M. *Inorg. Chim. Acta* **2000**, *300*−*302*, 1014.
(28) (a) Fujii, T.; Kodaira, K.; Kawauchi, O.; Tanaka, N.; Yamashita, H.; Anpo, M. *J. Phys. Chem. B* **1997**, *101*, 10631. (b) Shen, W. Y.; Pang, M. L.; Lin, J.; Fang, J. Y. *J. Electrochem. Soc.* **2005**, *152*, H25.
(29) Kahwa, I. A.; Selbin, J.; O'connor, C. J.; Foise, J. W.; McPherson, G. L. *Inorg. Chim. Acta* **1988**, *148*, 265.
(30) Kahn, M. L.; Sutter, J.-P.; Golhen, S.; Guionneau, P.; Ouahab, L.; Kahn, O.; Chasseau, D. *J. Am. Chem. Soc.* **2000**, *122*, 3413.
(31) Kahn, O. *Molecular Magnetism*; VCH: New York, 1993.
(32) Andruh, M.; Bakalbassis, E.; Kahn, O.; Trombe, J. C.; Porcher, P. *Inorg. Chem.* **1993**, *32*, 1616.
(33) (a) Sorace, L.; Benelli, C.; Gatteschi, D. *Chem. Soc. Rev.* **2011**, *40*, 3092. (b) Habib, F.; Lin, P.-H.; Long, J.; Korobkov, I.; Wernsdorfer, W.; Murugesu, M. *J. Am. Chem. Soc.* **2011**, *133*, 8830. (c) Tang, J. K.; Hewitt, I.; Madhu, N. T.; Chastanet, G.; Wernsdorfer, W.; Anson, C. E.; Benelli, C.; Sessoli, R.; Powell, A. K. *Angew. Chem., Int. Ed.* **2006**, *45*, 1729. (d) Blagg, R. J.; Muryn, C. A.; Tuna, F.; McInnes, E. J. L.; Winpenny, R. E. P. *Angew. Chem., Int. Ed.* **2011**, *50*, 6530.